Annals of Biomedical Engineering, Vol. 22, pp. 280–292, 1994
Printed in the USA.

0090-6964/94 $10.50 + .00

A Fiber Matrix Model for Fluid Flow and Streaming Potentials in the Canaliculi of an Osteon

Y. ZENG, S.C. COWIN and S. WEINBAUM

Department of Mechanical Engineering, The City College of the City University of New York, New York, NY 10031

Abstract—A theoretical model is developed to predict the fluid shear stress and streaming potential at the surface of osteocytic processes in the lacunar-canalicular porosity of an osteon when the osteon is subject to mechanical loads that are parallel or perpendicular to its axis. The theory developed in Weinbaum *et al.* (31) for the flow through a proteoglycan matrix in a canaliculus is employed in a poroelastic model for the osteon. Our formulation is a generalization of that of Petrov *et al.* (17). Our model predicts that, in order to satisfy the measured frequency dependence of the phase and magnitude of the SGP in macroscopic bone samples, the fiber spacing in the fluid annulus must lie in the narrow range 6–7 nm typical of the spacing of GAG sidechains along a protein monomer. The model predictions for the local SGP profiles in the osteon agree with the experimental observations of Starkebaum *et al.* (24). The theory predicts that the pore pressure relaxation time, τ_d, for a 150–300 μm diameter osteon with the foregoing matrix structure is approximately 0.03–0.13 sec, and that the amplitude of the mean fluid shear stress on the membrane of the osteocytic process at the mean areal radius of the osteon has a maximum at 28 Hz if $\tau_d = 0.06$ sec. This maximum, which is independent of the magnitude of the loading, could be important *in vivo* since the recent experiments of Turner *et al.* (28) and McLeod *et al.* (15) have a peak in the strain frequency spectrum between 20 and 30 Hz that also appears to be independent of the type (magnitude) of loading. Numerical predictions for the amplitude of the average fluid shear stress on the osteocytic membrane at the mean areal radius of the osteon show that the fluid shear stress associated with the low amplitude 20–30 Hz spectral strain component is at least as large as the average fluid shear stress associated with the high amplitude 1 Hz stride component, although the latter loading is an order of magnitude larger, and has a magnitude that lies within the middle of the range, 6–30 dynes/cm^2, where fluid shear stresses in tissue culture studies with osteoblast monolayers have elicited an intracellular Ca^{++} response (31). The implications of these results for intracellular electrical communication are discussed.

Keywords—Osteon, Canaliculi, Streaming potentials, Fiber matrix, Osteocytes, Fluid shear stress.

Acknowledgment—This research is supported by NASA Grant NAGW-3860.

Address correspondence to S. Weinbaum, Department of Mechanical Engineering, The City College of the City University of New York, New York, NY 10031.

(Received 29Nov93, Revised 25Feb94, Accepted 9Mar94)

INTRODUCTION

In this paper, we develop a theoretical model to describe the fluid flow and the strain-generated potential (SGP) in the lacunar-canalicular porosity of an osteon under sinusoidal loading that is either perpendicular or parallel to the axis of the osteon. This model is intended to predict the location dependence and magnitude of the SGP that were measured in the pioneering study by Starkebaum *et al.* (24), in which the detailed measurements of the SGP around individual osteons were correlated with bone morphology. The model is also used to analyze the structure of the proteoglycan matrix in the fluid space surrounding the osteocytic process in the canaliculus and to relate this structure to the fluid shear stress on the cell membrane of the osteocytic process for mechanical loadings that are typical of those produced in the long bones of human and animal limbs due to either a cyclic loading of 1,000–2,000 μ strain associated with the fundamental 1–2 Hz stride frequency or 100–200 μ strain associated with the high frequency 20–30 Hz spectral component that was observed during standing or normal gait McLeod *et al.* (15).

The experimental study by Starkebaum *et al.* (24) revealed several essential features of the osteonal-related SGP. It showed that the local osteonal field was 10 to 30 times greater than the background field associated with the SGP across the entire bone specimen, was nearly axisymmetric, and had a cusp-like shape that changed direction from the tension to the compression side of the specimen. The present model for predicting these basic features draws heavily upon an earlier formulation and numerical solution by Petrov *et al.* (17) and two recent papers by the authors, Weinbaum *et al.* (31) and Cowin *et al.* (5). In (17), the electrokinetic theory in Salzstein *et al.* (22), which was previously developed to predict the phase and magnitude of the macroscopic SGP across the entire bone specimen, was applied to an individual osteon and a numerical solution obtained for the boundary value problem associated with the pore pressure of this osteonal system. This formulation assumed that the SGP was associated with the fluid flow in a system of 10 to 35 nm radius pores associated with collagen-hydroxyapatite porosity.

The present analysis, while closely resembling the formulation in Petrov *et al.* (17), differs in the description of the interstitial fluid flow at the microstructural level and the anatomical structures that determine this flow. It assumes that, in contrast to the view in Salzstein *et al.* (22), the SGP is generated in the lacunar-canalicular porosity and that the fluid resistance arises from hydrodynamic forces on the boundaries of the fluid annulus that surrounds the osteocytic processes, *i.e.*, the cell membrane of the osteocytic process, the walls of the canaliculi and, most importantly, the proteoglycan matrix associated with the membrane surface of the osteocytic process. This new view and its physiological implications are described in much greater depth in two recent papers by the authors (5,31). The essential features as they relate to the present study are summarized in the next section.

BACKGROUND

Although many investigators have examined various aspects of convective flow in the lacunar-canalicular porosity (9,12,18), the lacunar-canalicular porosity has not been associated with the relaxation of the excess pore pressure and the SGP until recently. The reason for the failure to associate the lacunar canalicular flow with the SGPs was that the measured relaxation time for the SGP in one mm thick specimens was two orders of magnitude larger than estimates of the drainage time for the canaliculi, assuming the latter were simple pores devoid of cellular and fiber matrix components. In Weinbaum *et al.* (31) the Biot and Darcy-Brinkman theories are combined to describe the presence of the osteocytic processes and gel-like proteoglycan structures in the fluid annulus. In the latter study, the fiber spacing parameter, Δ, was chosen as 7 nm, a value that is characteristic of the spacing of GAG sidechains of a protein monomer if the latter is ordered by albumin. For this prescribed value of Δ, the theory is able to predict accurately the measured relaxation time, 1–2 sec, of the macroscopic SGP. In (5), this theory is extended to show that the frequency dependence of the phase and magnitude of the SGP that is measured in the 4-point bending apparatus experiments of Salzstein *et al.* (23) and Scott and Korostoff (25) can also be predicted by this new model if Δ = 6-7 nm and q, the ratio of the radius of the canaliculus to the radius of the osteocytic process, is approximately 3. In the present study, instead of prescribing Δ, we will examine how the relaxation time and phase of the SGP in an osteonal system change as the fiber spacing (*i.e.*, the characteristic spacing of GAG sidechains) is varied between 4 and 20 nm.

An important aspect of the new model in Weinbaum *et al.* (31) is that it can be used to predict the maximum fluid shear stress on the membranes of the osteocytic processes. It is shown that, for Δ = 6-7 nm and q = 2, the maximum shear stress on trabecular elements for physiological loading conditions corresponding to either the 1–2 Hz fundamental stride or high frequency 20–30 Hz spectral strain components lie within a range where cultured osteoblast monolayers have been demonstrated to release intracellular Ca^{++} Williams *et al.* (32) and second messengers Reich and Frangos (20). Intracellular Ca^{++} is believed to regulate the opening and closing of the hydrophilic pores in the gap junction proteins that link the apical ends of osteocytic processes of neighboring osteocytes as well as osteoblasts at the bone surface, and thus control the intracellular ionic currents that pass through the gap junction proteins of the interconnected cell network. This combination of model predictions and physical reasoning has led to a new hypothesis in (30) for the cellular level mechanosensory mechanism by which bone cells sense mechanical strain and communicate this physical loading to the osteoblasts at the bone surface. In the present study, we will also examine how the fluid shear stress on the membranes of the osteocytic processes varies in individual osteons as a function of canalicular geometry and proteoglycan matrix structure for physiological loads representative of either the fundamental stride or the 20–30 Hz spectral strain component.

MATHEMATICAL FORMULATION

The presentation of the formulation and solution of the single osteon problem addressed in this study is divided into four subsections: the flow in the canaliculus, the poroelasticity theory to determine the pore pressure in the osteon, the electrokinetic theory to determine the SGP, and the calculation of the fluid shear stress on the osteocytic process. Results derived in (5,17,31) will be used directly, where possible, with appropriate references given.

Flow in Canaliculi

The formulation and solution of the boundary value problem for the flow through the gel-like proteoglycan structure in the fluid annulus that surrounds the osteocytic process in the canaliculus is given in (31). We present below only the essential features of this formulation and solution required for our single osteon model. In (31), three hierarchical levels of permeability are introduced: the smallest scale is associated with the open spacing, Δ, between GAG fibers; the intermediate scale is associated with thickness of the fluid annulus, $b - a$; and the largest scale is associated with the Darcy permeability constant that appears in the Biot equation governing the fluid pore pressure. The smallest scale permeability constant, k_p, appears in the Darcy-Brickman equation,

$$\nabla p = -\frac{\mu}{k_p}\,\mathrm{u} + \mu\,\nabla^2\,\mathrm{u}, \qquad (1)$$

for the fluid flow in the fiber filled annulus surrounding the osteocytic process. For an ordered matrix of parallel fibers, k_p is given in Tsay and Weinbaum (28) as

$$k_p = 0.0572\, a_0^2 \left(\frac{\Delta}{a_0}\right)^{2.377}, \tag{2}$$

where a_0 is the fiber radius and $2a_0 + \Delta$ is the fiber spacing. Eq. 2 is a reasonable quantitative approximation for flow either perpendicular or parallel to the fiber array. In (28), it is shown that the effective medium approach given by Eq. 1 is highly accurate for slender fibers whose length-to-diameter ratio is greater than 5. This criterion is well satisfied by the GAG sidechains in a proteoglycan matrix.

The solution of Eq. (1) for the velocity profile in the fluid annulus is given as

$$u = \frac{k_p}{\mu}\frac{\partial p}{\partial r}\left[A_1 I_0\left(\gamma\frac{\rho}{b}\right) + B_1 K_0\left(\gamma\frac{\rho}{b}\right) - 1\right], \tag{3}$$

where the canalicular axis lies along the osteonal radial coordinate r, ρ is a radial coordinate measured from $\rho = a$, the radius of the osteocytic process, to $\rho = b$, the wall of the canaliculus and

$$A_1 = \frac{K_0(\gamma) - K_0(\gamma/q)}{I_0(\gamma/q)K_0(\gamma) - I_0(\gamma)K_0(\gamma/q)},$$
$$B_1 = \frac{I_0(\gamma/q) - I_0(\gamma)}{I_0(\gamma/q)K_0(\gamma) - I_0(\gamma)K_0(\gamma/q)}. \tag{4}$$

Here K_0 and I_0 are modified Bessel functions of zeroth order, $q = b/a$ and $\gamma = b/\sqrt{k_p}$. The pressure gradient, $(\partial p)/(\partial r)$ in Eq. (3) is along the axis of the canaliculus and is determined by the solution, given in the next subsection, of the pore pressure distribution in the osteon.

Eq. 3 for the velocity u can be written in a much simpler form for the limiting case when the fiber matrix is very dilute, *i.e.*, k_p tending to infinity. In this case, Eq. 3 reduces to the solution of the Stokes equation for the flow in an annulus

$$u_\infty = \frac{a^2}{4\mu}\frac{\partial p}{\partial r}\left[\frac{\rho^2}{a^2} - 1 - \left(\frac{q^2 - 1}{\ln q}\right)\ln\frac{\rho}{a}\right], \tag{5}$$

where u_∞ is the velocity in the dilute fiber limit.

The shear stress acting at the inner surface of the annular region (the exterior surface of the membrane of the osteocytic process), is readily obtained from the gradient of the velocity profile in Eq. 3 by evaluating it at $r = a$,

$$s(a) = \mu\frac{\partial u}{\partial \rho}(a) = \frac{b}{\gamma}\frac{\partial p}{\partial r}\left[A_1 I_1(\gamma/q) - B_1 K_1(\gamma/q)\right]. \tag{6}$$

In the dilute fiber limiting case, Eq. 6 reduces to the inner wall shear stress for Stokes flow in an annulus, which we indicate by $s(a)_\infty$,

$$s(a)_\infty = \mu\frac{\partial u}{\partial \rho}(a) = \frac{a}{2}\frac{\partial p}{\partial r}\left(1 + \frac{1 - q^2}{2\ln q}\right). \tag{7}$$

From Eqs. 6 and 7, the ratio of the shear stress on the osteocytic membrane in the case when the fiber matrix components in the annulus are present to the case when they are absent is given by

$$\frac{s(a)}{s(a)_\infty} = \frac{2q}{\gamma}\frac{A_1 I_1(\gamma/q) - B_1 K_1(\gamma/q)}{1 + (1 - q^2)/2\ln q}. \tag{8}$$

The large-scale permeability constant, k, is obtained by first integrating Eq. 3 to determine the fluid flux in a single annulus and then multiplying this flux by the number of canaliculi per unit area, n. The final expression for the Darcy large-scale permeability that will appear in the diffusion constant, c, in the partial differential equation (Eq. 11) governing the diffusion of the pore water pressure is

$$k = \frac{2\pi n a^4 q^3}{\gamma^3}\left\{A_1[I_1(\gamma/q) - qI_1(\gamma)] + B_1[qK_1(\gamma) - K_1(\gamma/q)] + \frac{\gamma(q^2 - 1)}{2q}\right\}. \tag{9}$$

The results described above are derived in (31).

Pore Pressure in an Osteon

The formulation of the boundary value problem to determine the pore pressure in a single osteon closely follows that presented in (17). The simplifying assumptions, boundary conditions and governing equations for the pore pressure are the same. The present analysis differs from this earlier study in three ways. First, the Darcy permeability, k, is given by effective medium theory for flow in the canaliculi, (Eq. 9), as opposed to a simple pore theory. Second, closed-form analytic solutions are obtained for the pore pressure, in contrast to the earlier work by Petrov *et al.* (17) where the boundary value problem was solved numerically. Third, we consider the physiological case where an osteon is loaded along its axis in addition to the experimental situation of Starkebaum *et al.* (24), in which only the loading transverse to the osteonal axis was considered.

Poroelasticity (Biot theory) is the model used for calculating the local fluid pressure gradient in the canaliculus from the externally applied load. First, we consider 2-D loading. For an osteon under sinusoidal loading perpendicular to the axis of the osteon, the stress field of an

infinite plate containing a circular hole of radius, r_i, that represents the osteonal lumen is given by

$$T_{kk} = T_{rr} + T_{\theta\theta} = S\left[1 - \left(\frac{2r_i^2}{r^2}\right)\cos 2\theta\right], \quad (10)$$

where $S = -\sigma_0 - \sigma \sin \omega t$, Timoshenko and Goodier (27, p. 91). When the applied stress field given by expression (10) is inserted into the partial differential equation for the pore pressure (obtained from poroelasticity theory), one obtains

$$\frac{\partial^2 p}{\partial r^2} + \frac{1}{r}\frac{\partial p}{\partial r} + \frac{1}{r^2}\frac{\partial^2 p}{\partial \theta^2} - \frac{1}{c}\frac{\partial p}{\partial t} = -\frac{\sigma\omega B}{3c}\cos\omega t\left[1 - \left(\frac{2r_i^2}{r^2}\right)\cos 2\theta\right], \quad (11)$$

where B ($B = 0.53$) is a factor representing the relative compressibility of bone matrix and bone water and c is a diffusion constant defined by Eq. 19 in Weinbaum et al. (31). The expression for c is given by (k/μ) $(13.5GPa)$, where the large-scale permeability constant, k, in turn, is given in Eq. 9.

The differential equation (Eq. 11) is rendered dimensionless by the introduction of the dimensionless variables,

$$R = \frac{r}{r_o},\ \tau = \frac{ct}{r_o^2},\ P = \frac{3p}{\sigma BT},\ T = \frac{\omega r_o^2}{c},\ R_i = \frac{r_i}{r_o}; \quad (12)$$

thus,

$$\frac{\partial^2 P}{\partial R^2} + \frac{1}{R}\left(\frac{\partial P}{\partial R}\right) + \frac{1}{R^2}\frac{\partial^2 P}{\partial \theta^2} - \frac{\partial P}{\partial \tau} = -\cos T\tau\left[1 - \frac{2R_i^2}{R^2}\cos 2\theta\right]. \quad (13)$$

The first three of the dimensionless quantities introduced in Eq. (12) render the length, time, and pressure variables dimensionless. The dimensionless frequency parameter, T, is the ratio of the characteristic time of relaxation of the fluid pore pressure, $\tau_d = r_o^2 c^{-1}$, to the characteristic time of applied forcing, $\tau_f = \omega^{-1}$; T is small when $\tau_d \ll \tau_f$ and large when the reverse is true. The characteristic time of decay of the fluid pore pressure is related to the large-scale permeability constant, k,

$$\tau_d = \frac{r_o^2}{c} = \frac{\mu r_o^2}{k(13.5GPa)}, \quad (14)$$

where k is given in Eq. 9.

The boundary conditions used for the solution of Eq. 13 are

$$P = 0, \qquad \text{at } R = R_i = \frac{r_i}{r_o}, \quad (15a)$$

$$\frac{\partial P}{\partial R} = 0, \qquad \text{at } R = 1. \quad (15b)$$

The boundary condition in Eq. 15b is an approximation which requires that the flow through the cement line of the osteon at r_o be negligible compared with the flow at r_i, the Haversian canal. The solution of Eq. 13 subject to Eq. 15 is

$$P = \frac{1}{T}\mathrm{Re}\{e^{iT\tau}[A_0 I_0(\sqrt{iT}\,R) + B_0 K_0(\sqrt{iT}\,R) + (A_2 I_2(\sqrt{iT}\,R) + B_2 K_2(\sqrt{iT}\,R))\cos 2\theta]\} + \frac{1}{T}\left(1 - \frac{2R_i^2}{R^2}\cos 2\theta\right)\sin T\tau, \quad (16)$$

where

$$A_0 = \frac{iK_1(\sqrt{iT})}{I_0(\sqrt{iT}\,R_i)K_1(\sqrt{iT}) + I_1(\sqrt{iT})K_0(\sqrt{iT}\,R_i)}, \quad (17a)$$

$$B_0 = \frac{iI_1(\sqrt{iT})}{I_0(\sqrt{iT}\,R_i)K_1(\sqrt{iT}) + I_1(\sqrt{iT})K_0(\sqrt{iT}\,R_i)}, \quad (17b)$$

$$A_2 = -i2R_i^2\left[\frac{2}{\sqrt{iT}}\left(K_2(\sqrt{iT}R_i) - \frac{1}{R_i^2}K_2(\sqrt{iT})\right) - \frac{1}{R_i^2}K_1(\sqrt{iT})\right]/\Delta_2, \quad (17c)$$

$$B_2 = i2R_i^2\left[\frac{2}{\sqrt{iT}}\left(I_2(\sqrt{iT}R_i) - \frac{1}{R_i^2}I_2(\sqrt{iT})\right) + \frac{1}{R_i^2}I_1(\sqrt{iT})\right]/\Delta_2, \quad (17d)$$

and

$$\Delta_2 = -K_2(\sqrt{iT}\,R_i)I_1(\sqrt{iT}) - K_1(\sqrt{iT})I_2(\sqrt{iT}\,R_i) - \frac{2}{\sqrt{iT}}(K_2(\sqrt{iT})\,I_2(\sqrt{iT}) - I_2(\sqrt{iT})K_2(\sqrt{iT}\,R_i)).$$

For an osteon under sinusoidal loading parallel to the axis of the osteon, the dimensionless governing equation is

$$\frac{\partial^2 P}{\partial R^2} + \frac{1}{R}\left(\frac{\partial P}{\partial R}\right) + \frac{1}{R^2}\frac{\partial^2 P}{\partial \theta^2} - \frac{\partial P}{\partial \tau} = -\cos T\tau. \quad (18)$$

Note that this equation is the same as Eq. 13 without the cos2θ forcing term. The solution of Eq. 18 subject to Eq. 15 is a reduced form of Eq. 16 in which the azimuthal terms are absent:

$$P = \frac{1}{T}\,\mathrm{Re}\{e^{iT\tau}[A_0 I_0(\sqrt{iT}\,R) + B_0 K_0(\sqrt{iT}\,R)]\} + \frac{1}{T}\sin T\tau. \tag{19}$$

Stress Generated Potential

From Eq. 4 in Petrov *et al.* (17), the SGP in the lacunar-canalicular porosity of an osteon is, using Eqs. 16 and 19,

$$V_{\mathrm{SGP}} = \frac{F}{\sigma_f}p = \frac{F}{\sigma_f}\cdot\frac{\sigma BT}{3}P = \frac{\sigma BF}{3\sigma_f}(\sin T\tau + \mathrm{Re}\{e^{iT\tau}[A_0 I_0(\sqrt{iT}\,R) + B_0 K_0(\sqrt{iT}\,R)]\}) \tag{20}$$

for parallel loading, and

$$V_{\mathrm{SGP}} = \frac{\sigma BF}{3\sigma_f}\left[\left(1 - \frac{2R_i^2}{R^2}\cos 2\theta\right)\sin T\tau + \mathrm{Re}\{e^{iT\tau}[A_0 I_0(\sqrt{iT}\,R) + B_0 K_0(\sqrt{iT}\,R) + (A_2 I_2(\sqrt{iT}\,R) + B_2 K_2(\sqrt{iT}\,R))\cos 2\theta]\}\right] \tag{21}$$

for perpendicular loading. In these equations, σ_f is the electrical conductivity of the solution and F is a complicated electrokinetic coefficient, which is derived in Cowin *et al.* (5). This expression for F depends on the distribution of the ionic current in the fluid annulus surrounding the osteocytic process. This current distribution depends critically on the relative thickness of the Debye double layers and the fiber-induced boundary layers at the walls of the annulus. The final expression for F is given by Eq. 20 in Cowin *et al.* (5). The solution for V_{SGP} can be made dimensionless by introducing the factor, $(\sigma BF)/(3\sigma_f)$, which has the dimension of volts. The dimensionless SGP is

$$\overline{V}_{\mathrm{SGP}} = V_{\mathrm{SGP}}\Big/\left(\frac{\sigma BF}{3\sigma_f}\right). \tag{22}$$

Shear Stress on the Osteocytic Process

We first determined the magnitude of the maximum shear stress on the membrane surface of the osteocytic processes in a trabecula during a loading cycle. Eq. 6 gives the shear stress on the membrane surface of the osteocytic processes, and Eqs. 16 and 19 provide the dimensionless pressure distribution for an osteon subject to transverse and parallel loading, respectively. In either case, the solution for the pressure has a maximum gradient at the osteonal inner boundary at $R = R_i$; thus, the shear stress on the osteocytic processes will be greatest at this osteonal surface. We denote the maximum shear stress that occurs during the course of one temporal cycle on a membrane surface located at the position (R_i, θ) in the osteon as $s(a)_{\max}$, which from Eqs. (6), (16) or (19) is given by

$$s(a)_{max} = \max\left[\frac{\sigma Bb}{3\gamma r_o}(A_1 I_1(\gamma/q) - B_1 K_1(\gamma/q))\mathrm{Re}\{W\,e^{iT\tau}\}\right]_\theta, \tag{23}$$

where

$$W = U + iV = [A_0 I_1(\sqrt{iT}R_i) - B_0 K_1(\sqrt{iT}\,R_i)]\sqrt{iT} \tag{24}$$

for parallel loading, and

$$W = U + iV = [A_0 I_1(\sqrt{iT}\,R_i) - B_0 K_1(\sqrt{iT}\,R_i) + (A_2 I_2'(\sqrt{iT}R_i) + B_2 K_2'(\sqrt{iT}\,R_i))\cos 2\theta]\sqrt{iT} - \frac{4iR_i^2}{R^3}\cos 2\theta \tag{25}$$

for perpendicular loading. From Eq. 23, the shear stress will achieve its maximum value when $\mathrm{Re}\{We^{iT\tau}\}$ is at a maximum. The time, τ, in the loading cycle when this occurs is given by

$$\tau_{\max} = -\frac{1}{T}\tan^{-1}\frac{V}{U} \tag{26}$$

where U and V are obtained from Eqs. 24 or 25. Using Eq. 26, one can show that the maximum value of $\mathrm{Re}\{We^{iT\tau}\}$ is simply $\sqrt{U^2 + V^2}$.

In Weinbaum et al. (31), the fluid shear stress excitation hypothesis was explored using the maximum shear stress on a trabecula as the criterion for excitation. This is equivalent to results in Eqs. 23 to 26 for the osteon. For reasons which will be described at greater length in the Discussion, a physiologically more meaningful criterion might be the average shear stress at the mean areal radius, r_m. This radius is the radius that divides the annular region between the lumen, r_i, and the cement line, r_o, of the osteon into equal annular areas,

$$r_m = \sqrt{\frac{r_o^2 + r_i^2}{2}} = r_o\sqrt{\frac{1 + R_i^2}{2}} = r_o R_m. \tag{27}$$

If we denote the time-averaged magnitude of the fluid

shear stress on the membrane of the osteocytic process at the mean areal radius R_m by $s(a)_{m,av}$, then from Eqs. 6 and 19,

$$s(a)_{m,av} = \frac{T}{\pi}\int_0^{\frac{\pi}{T}} |s(a)|_{R=R_m}\, d\tau = \frac{2}{\pi}\frac{\sigma B b}{3\gamma r_o}\,[A_1 I_1(\gamma/q) - B_1 K_1(\gamma/q)]\,|W|_m, \tag{28}$$

where W is given by Eqs. (24) and (25) for parallel and transverse loading, respectively.

PARAMETER VALUES

The selection of the values of parameters a_0, a, n, q, and τ_d is discussed in detail in Cowin *et al.* (5) where the sensitivity of the solutions for the phase and magnitude of the SGP across the entire bone specimen to the key input parameters, q, n, and a is compared with the experimental measurements in Salzstein and Pollack (23) and Scott and Korostoff (25). In Cowin *et al.* (5), it was shown that close agreement with experiment could be obtained for both the phase and magnitude when q was approximately 2.0, $\tau_d = 1.42$ sec. for a 1 mm thick specimen, and $n = 20/(30\ \mu\text{m})^2 = 0.022\ \mu\text{m}^{-2}$ assuming that the radius of the osteocytic process, $a = 100$ nm, the fiber radius, $a_o = 1.0$ nm, and $\Delta = 6$ nm. The values of a and a_0 are well accepted values in the literature. The predicted values of q and n both fall within the range $1.5 \leq q \leq 3$ and $0.01 \leq n \leq 0.025\ \mu\text{m}^{-2}$, respectively, observed in morphometric studies.

The selection of Δ requires an assumption as to the structure of the GAG sidechains and a knowledge of the proteoglycans in the fluid annulus surrounding the osteocytic process. Whereas the collagen fibrils and proteoglycan components of the mineralized collagen-hydroxyapatite have been characterized (see Robey *et al.* [21]), the gel-like components of the fluid annulus that diffusely stain for horseradish peroxidase Doty *et al.* (6), osmium tetroxide Wasserman and Yaeger (30), and microperoxidase Tanaka and Sakamo (26) have yet to be either isolated or identified. The selection of Δ is thus the largest uncertainty in the model. However, reasonable bounds and a most likely estimate for Δ can be established by comparison with the matrix in other tissues.

In Weinbaum *et al.* (30) and Cowin *et al.* (5), we assumed that since albumin (effective diameter, 7 nm) was abundant in the plasma-derived bone fluid, this molecule ordered the GAG and formed a molecular sieve with Δ = 6–7 nm, as first proposed by Michel (16) for the surface glycocalyx of capillary endothelial cells perfused in plasma. Strong evidence in support of this hypothesis for capillary endothelium was recently obtained by Adamson and Clough (1) in which it was demonstrated that ferritin, a nearly spherical molecule 10 nm in diameter could not penetrate the ordered GAG of the surface proteoglycan layer if albumin were present in the perfusate. In contrast, in the absence of plasma proteins (pure Ringer perfusate), this layer was clumped and highly permeable to ferritin. In the present study, we will let Δ vary between 4 nm (the closest spacing suggested for the GAG in cartilage proteoglycan Buschman *et al.* [4]) and 20 nm (the largest value that has been suggested for the spacing of the chondroitan sulfate [CS] sidechains of the proteoglycan monomers of this common proteoglycan) and examine the effect of Δ on both pore pressure relaxation time and osteocytic membrane shear stress. In the mineralized bone compartment, a large CS proteoglycan (versican) is replaced by biglycan and decorin as mineralization proceeds Roby *et al.* (21). It is not presently known whether this replacement also occurs outside the mineralized region. This point is returned to in the Discussion.

RESULTS

The fluid shear stress, $s(a)$, on the membrane of the osteocytic process is a function of the fiber matrix parameters a_0 and Δ and the geometry of the canaliculus. The ratio, $s(a)/s(a)_\infty$ given by Eq. 8 is plotted as a function of Δ for several values of q in the physiological range 2–3 in Fig. 1. One observes that for $q > 2.5$, even the most dilute matrix considered, $\Delta = 20$ nm, leads to a decrease of one order of magnitude in shear stress from the case when no matrix is present. There is typically a more than five-fold decrease in $s(a)/s(a)_\infty$ as the spacing of the matrix is decreased from $\Delta = 20$ nm to the most likely estimate, Δ = 6–7 nm, in our earlier studies, and the sensitivity to q in

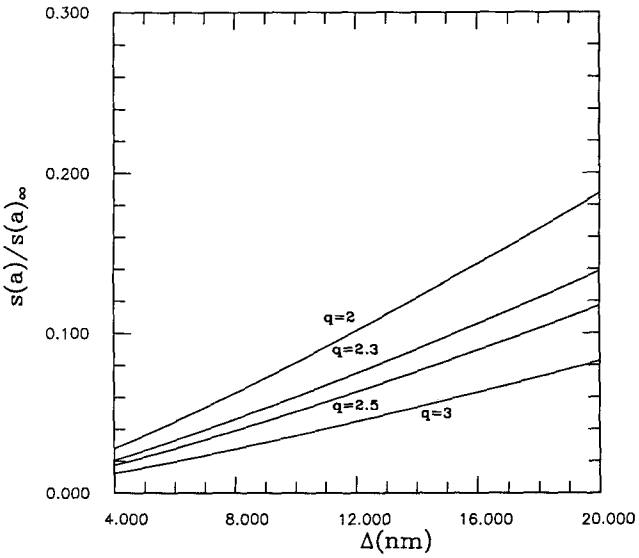

FIGURE 1. The shear stress ratio $s(a)/s(a)_\infty$, Equation (8), plotted against the fiber spacing parameter Δ for q = 2, 2.3, 2.5 and 3. a_0 = 1.0 nm and a = 100 nm. Note this ratio is independent of the loading (pore pressure gradient).

the most likely physiological range, $2 < q < 2.5$, is small.

The theoretical prediction made in Eq. 14 for the characteristic time of decay of the pore pressure in the osteon τ_d is shown in Fig. 2 for the same values of q and Δ as appear in Fig. 1. There is an order of magnitude decrease in τ_d as Δ is increased from 6 to 20 nm. The characteristic relaxation time for an osteon 200 μm in diameter is of the order 0.02 to 0.06 sec for $\Delta = 6$ nm. This characteristic time is a factor of 25 smaller than the decay time for the macroscopic SGP across the entire 1 mm thick specimen (the τ_d for the 1 mm thick specimen is obtained by replacing r_o in Eq. 14 by the specimen half thickness, d).

The variation of the dimensionless peak SGP of an osteon along radii at θ equal to 0 and π/2 is shown in Fig. 3 for three loading frequencies, $\omega = 1$ Hz and $\omega = 20$ Hz, typical of the stride and the high frequency spectral response observed in Turner *et al.* (29) and McLeod *et al.* (15), and also for $\omega = 100$ Hz. This calculation, based on Eqs. 21 and 22, assumes that $q = 2$, $\Delta = 6$ nm and that $r_i = 27$ μm. It follows from Fig. 2 that $\tau_d = 0.057$ sec for $q = 2$ and $\Delta = 6$ nm. One observes that there is only a relatively small azimuthal asymmetry in the SGP, as noted previously, in the numerical solution of Petrov *et al.* (17) and the measurements of Starkebaum *et al.* (24) except at very high frequency, $\omega = 100$ Hz. The important observation in Fig. 3 is that there is a large increase in magnitude of $\bar{V}_{SGP}$ when $\omega > 1$ Hz, that the maximum $\bar{V}_{SGP}$ is achieved for ω of order 100 Hz and that $\omega = 20$ Hz is near the center of this large increase in the stress generated potential. This result gives rise to a maximum in the pressure gradient and fluid shear stress at the mean areal radius

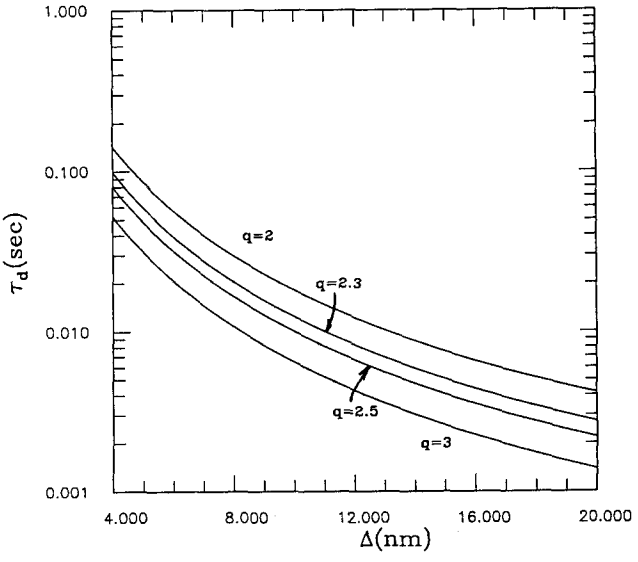

FIGURE 2. The characteristic draining time τ_d plotted as a function of fiber spacing Δ for $q = 2, 2.3, 2.5$, and 3. The values for the parameters employed were $n = 20/(30\ \mu m)^2$, $a_0 = 1.0$ nm, $a = 100$ nm, and μ was taken to be the viscosity of water. This is a plot of equation (14) for τ_d using expression (2) for k_p.

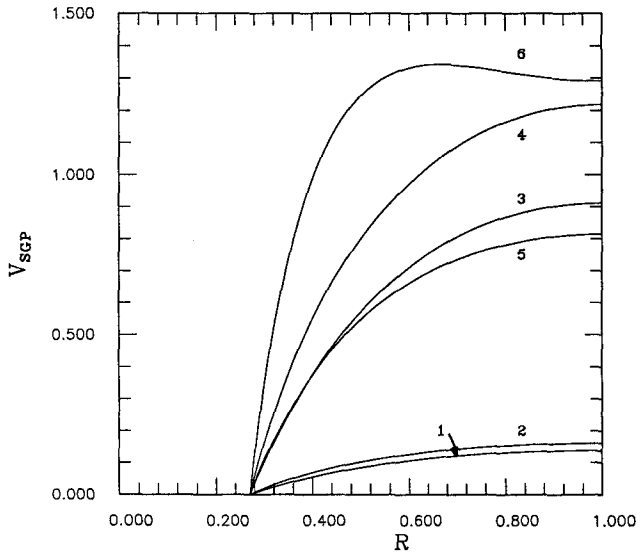

FIGURE 3. Plot of the peak solution profiles for $\bar{V}_{SGP}$, obtained from Eq. 22, as a function of the dimensionless radial distance R. $\tau_d = 0.057$ sec for all curves. Curves 1, 3, and 5 are for θ = 0 (horizontal axis) and curves 2, 4, and 6 are for θ = π/2 (vertical axis). Curves 1 and 2, 3 and 4, and 5 and 6 are for 1 Hz, 20 Hz, and 100 Hz, respectively.

of the osteon in the 20–30 Hz range of the frequency spectrum. This will be discussed later.

The radial $P = \bar{V}_{SGP}/T$ profiles are plotted in Fig. 4a for $\omega = 1$ Hz and Fig. 4b for $\omega = 20$ Hz at 45° increments in the phase of the loading for parallel loading and show the experimentally observed reversal in the cusp-like shape of the SGP from the compression to the tension side. Note that $P = \bar{V}_{SGP}/T$ has been plotted as the ordinate since the amplitude of this scaled pressure is of $O(1)$ for all frequencies, in contrast to $\bar{V}_{SGP}$ whose magnitude changes dramatically for frequencies greater than 1 Hz as observed in Fig. 3. At $\omega = 1$ Hz the phase of the loading is nearly 90° out of phase with the maximum in the $\bar{V}_{SGP}/T$ whereas at $\omega = 20$ Hz this phase has shifted ~70° and the maximum $\bar{V}_{SGP}$ profile lags the applied loading by only 20°. The peak SGP profile in Fig. 3 for $\omega = 20$ Hz is therefore lies above the 45° profile for $\bar{V}_{SGP}/T$ in Fig. 4b.

Inspection of the dimensionless solutions Eqs. 20 and 21 for the SGP and the coefficients that appear in these solutions reveals that for a given osteonal geometry the dimensionless solutions for V_{SGP}, Eq. 22, depend on only a single parameter, T, the dimensionless frequency parameter defined in Eq. 12. This frequency parameter, $T = \omega\tau_d$, is a function of the size of the osteon r_o and the canalicular geometry and matrix parameters, q and Δ, that appear in the effective large-scale Darcy permeability coefficient, k, in Eq. 9. k and r_o are the two parameters that determine τ_d, see Eq. 14. At any given position within the osteon, one could plot the shift in the phase angle of the SGP as a function of the dimensionless frequency param-

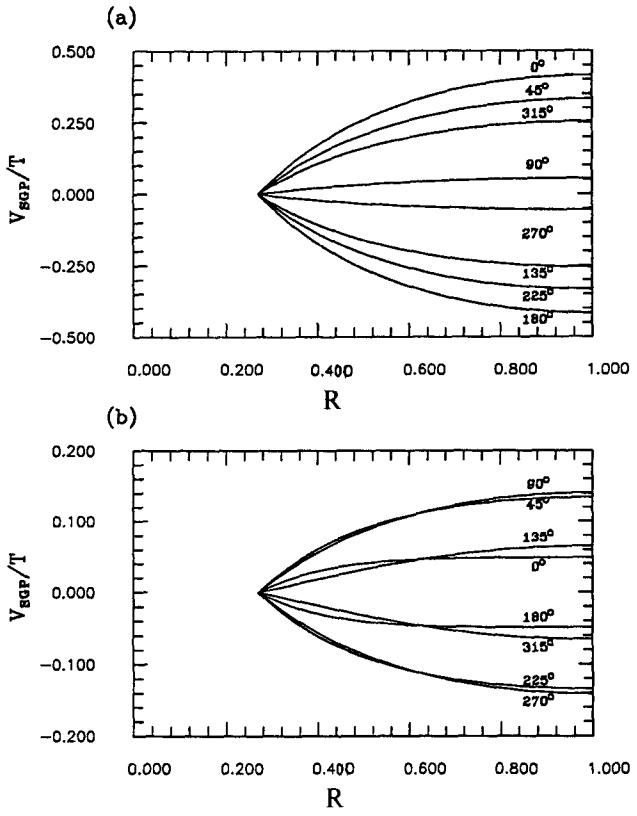

FIGURE 4. Plot of dimensionless pressure P or scaled SGP, $\bar{V}_{SGP}/T$, for parallel loading equation (19). τ_d = 0.057 sec. (a) ω = 1 Hz at 45° increments in phase ωt; (b) ω = 20 Hz at 45° increments in phase ωt.

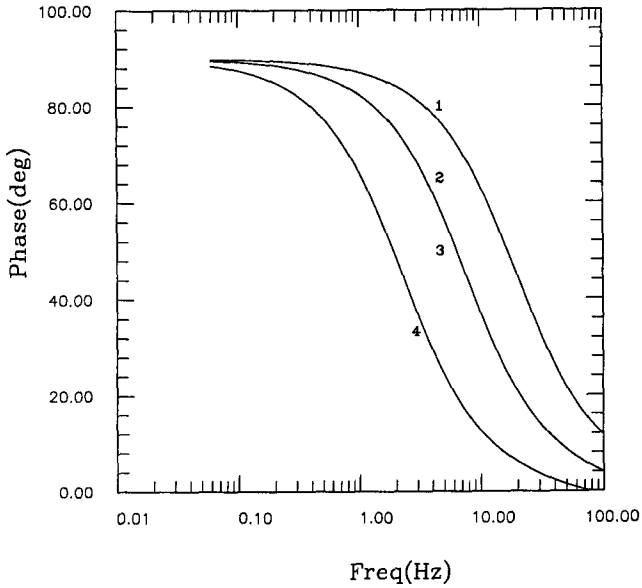

FIGURE 5. A plot of the phase angle of $\bar{V}_{SGP}$, obtained for parallel loading from Eq. (22) against frequency at τ_d = 0.032 sec (Curve 1), 0.057 sec (Curves 2 and 3) and 0.128 sec (Curve 4). This corresponds to osteonal outer radii r_o of 75, 100, and 150 μm, respectively, if q = 2 and Δ = 6 nm. Curves 1, 2, and 4 are plotted at $r = r_m$. Curve 3 is plotted at $r = r_0$.

eter, T, but this would not easily show the sensitivity of the results to variations in the parameters that determine τ_d which are shown in Fig. 2.

We have thus plotted in Fig. 5 the frequency response of the phase for three values of τ_d; 0.032, 0.057, and 0.128 sec. For q = 2 and Δ = 6 nm, these values of τ_d correspond to osteons whose diameter increases from 150 to 200 to 300 μm. Using the results in Fig. 2, one can also hold r_o fixed but vary q and Δ to obtain the three prescribed values of τ_d. For the osteon 200 μm in diameter the shift in phase is shown along the vertical line $\theta = \pi/2$ at both r_i and r_m for transverse loading. One observes that the phase varies very little with position within the osteon. Thus for osteons of 150 and 300 μm in diameter we have plotted the frequency response only at r_m for the case of parallel loading where the θ dependence is not present. Note that there is little shift in phase angle in all cases for loading frequencies less than 1 Hz and that the phase angle is approximately 20° for ω = 20 Hz for the 200 μm diameter osteon as observed in Fig. 4b.

The variation of the maximum fluid shear stress $s(a)_{max}$ (Curves 1 and 2) and the average fluid stress at the mean areal radius of the osteon $s(a)_{m,av}$ (Curves 3 and 4) with fiber spacing is shown in Fig. 6 where a, a_0, q, Δ, and r_o have the same values as Fig. 3. Curves 2 and 4 are for ω = 1 Hz and Curves 1 and 3 for 20 Hz. The maximum shear stress always occurs at the luminal surface of the osteon, where the pressure or potential field gradient is maximum as is evident from Fig. 3. It is important to point out that the applied cyclic load for the 20 Hz high frequency spectral strain is a factor of ten lower than the load of σ = 20 M Pa for the 1 Hz loading due to stride. This ratio is typical of the measurements in McLeod *et al.* (15) where the high frequency 20–30 Hz spectral strain component during standing or gait was 5 to 15% that of the fundamental mode due to stride. Despite this order of magnitude difference in amplitude one observes that the high frequency spectral component produces a maximum shear stress at the osteonal luminal border and an average fluid shear stress at the mean areal radius which is roughly 50% greater than the fundamental mode due to stride for all fiber spacings or equivalently, all values of τ_d. Similar results were observed in (31) for the maximum fluid shear stress at the surface of a simplified one-dimensional model for a plate-like trabecular element in combined bending and axial load.

The variation of $s(a)_{max}$ and $s(a)_{m,av}$ with frequency is shown in Fig. 7. The curves all assume a constant applied load amplitude of σ = 20 *M Pa* typical of the measured strains for the 1–2 Hz spectral component McLeod *et al. (15). Curves 1, 2, and 3 for* $s(a)_{max}$, which indicate the maximum shear stress on the membranes of the osteocytic

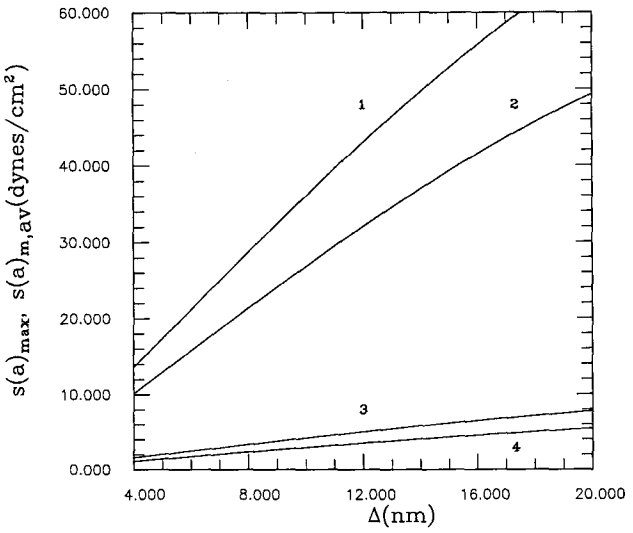

FIGURE 6. A plot of the maximum shear stress $s(a)_{max}$ at $r = r_i$ and the average shear stress $s(a)_{m,av}$ at $r = r_m$ on the membrane surface of the osteocytic processes, as a function of fiber spacing parameter, Δ, at the inner radius r_i and at the mean areal radius r_m of the osteon under parallel loading. The values of parameters are a_0 = 1.0 nm, a = 100 nm, and τ_d = 0.057 sec. Curve 1; $s(a)_{max}$ for ω = 20 Hz, σ = 2 *M Pa*. Curve 2; $s(a)_{max}$ for ω = 1 Hz, σ = 20 *M Pa*. Curve 3; $s(a)_{m,av}$ for ω = 20 Hz, σ = 2 *M Pa*. Curve 4; $s(a)_{m,av}$ for ω = 1 Hz, σ = 20 *M Pa*.

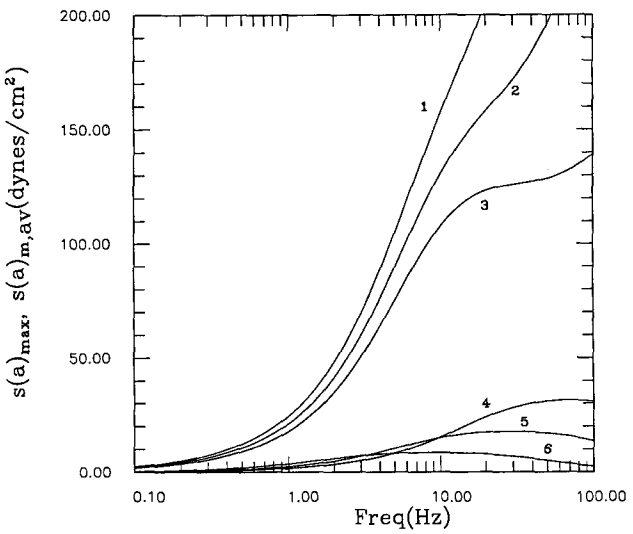

FIGURE 7. A plot of the average shear stress $s(a)_{m,av}$ at $r = r_m$ and the maximum shear stress $s(a)_{max}$ at $r = r_i$ on the membrane surface of the osteocytic processes, as a function of frequency ω. The Curves 1, 2, and 3 are for $s(a)_{max}$ and are plotted for parallel loading, Curve 2, and transverse loading, Curve 1 (θ = π/2) and Curve 3 (θ = 0). The average shear stress $s(a)_{m,av}$ is shown in Curves 4, 5, and 6 which correspond to τ_d = 0.032, 0.057, and 0.128 sec, or equivalently, osteonal diameters of 200, 300, and 400 μm, respectively, if q = 2 and Δ = 6 nm.

processes at the boundary with the osteonal canal, have been plotted for both parallel and transverse loading assuming that $\tau_d = 0.057$ sec. If we require that $q = 2$ and $\Delta = 6$ nm, as described previously in our discussion of parameter values, $r_o = 100$ μm. One observes that for ω > 10 Hz there is a significant azimuthal asymmetry in $s(a)_{max}$ as θ is increased from 0°, Curve 3, to 90°, Curve 1, for the transverse loading and these results bracket Curve 2 for parallel loading. Curves 4, 5 and 6 for $s(a)_{m,av}$ have been plotted only for parallel loading, but for three values of τ_d, 0.032, 0.057 and 0.128 sec corresponding to 150, 200, and 300 μm diameter osteons if $q = 2$ and $\Delta = 6$ nm. In contrast to the curves for $s(a)_{max}$, which show a rapid monotonic increase in fluid shear stress above 1 Hz, the curves for $s(a)_{m,av}$ show a rapid rise starting at 1 Hz, but then a monotonic decay at very high frequencies. This produces a maximum average shear stress at the mean areal radius of the osteon whose location shifts to the left in the figure as the size of the osteon or τ_d increases. For $\tau_d = 0.57$ sec the maximum is at 28 Hz. The origin of this maximum can be deduced from Fig. 3, where the profiles of $\bar{V}_{SGP}$, or equivalently the pore pressure, are plotted. At $\omega = 1$ Hz, $T \ll 1$ and there is enough time for the pore pressure to be relieved by fluid drainage into the Haversian canal. Thus $\bar{V}_{SGP} \ll 1$. For $\omega \gg 1$ Hz, or $T \gg 1$, $\bar{V}_{SGP}$ asymptotes to a maximum value and only the fluid near the Haversian canal has a chance to drain. There is relatively little fluid movement in the interior regions of the osteon. The maximum response is thus achieved for T of $O(1)$. We believe this intriguing behavior has important physiological implications that are related to both the 20–30 Hz peak strain component observed in the experiments of McLeod *et al.* (15) and the mechanosensory transduction mechanism proposed in Weinbaum *et al.* (31) (see Discussion).

DISCUSSION

A fundamental premise in our model is that the relaxation of excess pore pressure in an individual osteon and the associated SGP occur in the lacunar-canalicular porosity as opposed to pores in the mineralized collagen-hydroxyapatite, as concluded in Salzstein *et al.* (22) and Petrov *et al.* (17). The same arguments advanced in Cowin *et al.* (5) for the relaxation of the pore pressure and the associated SGP in the macroscopic bone sample also apply at the local level of a single osteon. The experiments by Tanaka and Sakano (26), which examine the penetration of microperoxidase MP (2 nm diameter) in the alveolar bone of five-day-old rats, provide convincing evidence for the lacunar-canalicular porosity being the site of the streaming current associated with the SGP. The electron micrographs in this study show a clear demarcation of MP at the interface between the mineralized and unmin-

eralized matrix with the MP being confined entirely to the lacunar-canalicular porosity and narrow regions of bone matrix bordering this porosity that still had not undergone mineralization. Since the size of the pores predicted in Salzstein *et al.* (22) (10 to 35 nm radius with an average of 16 nm) is far greater than the effective radius of the MP molecule (1 nm) hydrophilic pores in the mineralized matrix of these dimensions would have easily permitted the passage of this tracer molecule.

Figure 2 provides important insight into the likely structure of the proteoglycan matrix in the fluid annulus that surrounds the osteocytic process. Eq. 14 for τ_d is the same expression derived in Cowin *et al.* (5) to determine the pore pressure relaxation time for the macroscopic SGP, except that the characteristic length in the latter study was the half thickness (0.5 mm) of the entire bone specimen. The theoretical expression, Eq. 23 in (5) for V_{SGP}, which is used to curve fit data of Scott and Korostoff (25) for the change in phase of the SGP with frequency, depends only on the parameter τ_d in contrast to Eq. 20 for the single osteon where the phase depends not only on T but also on the osteonal geometry. A very close fit to the data in Scott and Korostoff (25) could be obtained in Cowin *et al.* (5) for $\tau_d = 1.42$ sec. This characteristic relaxation time was achieved by choosing $\Delta = 6$ nm and finding a compatible q that allowed a best fit for the change in magnitude of the SGP with frequency. This best fit was achieved for $q = 2$. τ_d for the single osteon for this combination of q and Δ is, from Fig. 2, 0.057 sec if $r_o = 100$ μm. However, Fig. 2 shows that there are other combinations of q and Δ that would allow τ_d to be 0.057 sec for a 200 μm diameter osteon or 1.42 sec for the macroscopic bone specimen. Anatomical studies indicate that q varies between 1.5 and 3, whereas the theoretical model in (5) predicts an even narrower range of q between 2 and 2.3, if one were also to obtain a reasonable curve fit for the variation of the magnitude of the experimentally measured SGP with loading frequency. For the anatomically observed range of $2 \leq q \leq 3$, Δ is constrained to the range between 3.8 and 6.0 nm, whereas for the more limited range of q, 2 to 2.3, predicted by the theory in (5), Δ is confined to the range approximately between 5 and 6 nm. The important point is that there is only a rather limited range of fiber spacings that are consistent with measured data for the frequency dependence of the SGP and anatomical observations for q.

The most likely range of Δ just predicted, 5–6 nm, corresponds roughly to the spacing of GAG sidechains in the proteoglycan matrix of other tissues. For example, our predicted Δ is comparable to the spacing of the GAG in nasal cartilage proteoglycan (chondroitan sulfate), which has been estimated to vary between 7 and 9 nm (3), and is also compatible with the observations of Adamson and Clough (1) for the size of the molecular sieve that limits the passage of ferritin (10 nm) through endothelial surface matrix. A related question is whether the matrix will fill the entire fluid annulus. The recent three-dimensional quick freeze-etch electron micrographs of ear cartilage reveal a continuity and attachment of the proteoglycan core protein to chondrocyte membrane, Mecham and Heuser (1990). A similar membrane attachment is observed for subendothelial matrix in arteries, Frank and Fogelman (1989). In both cases the proteoglycan has been identified as chondroitan sulfate (CS), where the length of the protein monomer is typically 300–400 nm. This type of core protein should easily fill the fluid annulus whose gap is only of the order of 100 nm.

Although the proteoglycans at the edge of the lacunar-canalicular border have been identified, the matrix in the fluid space of the canaliculus has not yet been characterized. From an evolutionary viewpoint, there is a possibility that this matrix may be a form of chondroitan sulfate. In the initial stages of bone formation, a large CS proteoglycan (versican) is found in the matrix surrounding osteoblasts and osteocytes. As mineralization proceeds, *in vivo* studies have shown a rapid migration to the mineralization front of a smaller mobile proteoglycan, biglycan (19), which is present in high concentration surrounding osteocytic lacunae (2). Deeper regions of the mineralized matrix contain primarily decorin (21). This suggests that in the fluid region surrounding the osteocytes, where no mineralization has occurred, no proteoglycan substitution has taken place and the primary proteoglycan that remains is the versican that was laid down initially. It is suggested in (21) that mineralization and proteoglycan substitution is prevented by calcium binding serum proteins, matrix proteins and crystal poisons that must first be removed for mineralization to proceed.

The only cell membranes where fluid shear stresses have been accurately measured or estimated on the basis of velocity measurements are vascular endothelial cells. Kamiya *et al.* (11) have shown that the average shear stress on the membranes of these cells is 15 to 20 dynes/cm^2 from the largest nutrient arteries to the arterial capillaries. Several investigators have performed experiments which have shown that when the flow into vessels is either increased or decreased there is an adaptive remodeling of the blood vessels to restore the fluid shear stress to the average range just cited (10,13); this adaptive response is lost if the endothelium is removed. The prediction of the maximum fluid shear stress on the membranes of the osteocytic processes at osteonal canal due to the 20–30 Hz spectral component is compatible with this measured range of shear stress for vascular endothelial remodeling. If we confine Δ to 6–7 nm for the reasons cited above, we can conclude from Fig. 6 that the maximum stress on the osteocytic membranes at $r = r_i$ for either the 1 Hz, 1,000 μ strain or the 20–30 Hz, 100 μ strain component falls in

the range 16 to 25 dynes/cm^2. One also observes from Fig. 1 that the shear stress would be more than an order of magnitude higher if matrix were not present in the fluid annulus. It is thus tempting to hypothesize that the fiber spacing of the matrix and the geometry of the canaliculus are coupled by design to maintain a shear stress on the osteocytic membranes, which is in approximately the same range as for vascular endothelium. This suggests that the osteocytes may release chemical substances that control the location of the mineralization front in a manner compatible with the shear stress at their surface.

The recent study by McLeod and Rubin (15) suggests that the strains associated with the 20–30 Hz loadings maintain bone mass at strain levels one order of magnitude lower than the strain levels necessary to maintain bone mass at 1 Hz. The principal controversy is whether these 20–30 Hz spectral components are due to muscular contractions. Turner *et al.* (29) maintain that the 25 Hz spectral component is also present during non-weight bearing conditions although, according to their experiments, the strain energy associated with the 20–30 Hz spectral components is increased twofold during locomotion. However, the predictions of our model and the validity of our fluid shear excitation hypothesis do not depend on the resolution of this controversy. Figure 6 shows that, whatever the origin of the low amplitude (100–200 μ strain) 20–30 Hz strain component, the membrane shear stresses that they produce are at least as large as those produced by the high amplitude (1,000–2,000 μ strain) 1 Hz low frequency stride component. Similar predictions for the relative magnitude of the fluid shear stresses induced by the 20–30 Hz and fundamental 1 Hz stride component were predicted for trabecular bone in (31).

If the 20–30 Hz spectral strain component is due to muscular contractions and these contractions are responsible for the maintenance of bone mass, as proposed in (15), then one expects that an intracellular biochemical response must be triggered in which osteocytes in the interior of the osteon first detect the mechanical load and are then able to communicate this information to the bone forming osteoblasts. The fluid shear stress excitation hypothesis proposed in (31) provides a rational explanation for this biosignaling behavior. First, the predicted amplitude range of the average strain-induced fluid shear stress at the inner radius of the osteon is in the middle of the range of fluid shear stresses, 6–30 dynes/cm^2, where intracellular calcium ions (32), and second messengers (20), have been released intracellularly in cultured monolayers of bone osteoblast and endothelial cells. Weinbaum *et al.* (32) have proposed that, since intracellular calcium is known to regulate the opening and closing of the hydrophilic pores in the transmembrane proteins of communicating junctions (14), and these junctions are the pathways for intracellular electrical currents, the fluid shear stress on the membranes of the osteocytic processes regulates the intracellular ion currents between cells and the latter is the cellular transduction mechanism by which osteocytes sense mechanical strain and communicate this information to osteoblasts, the cells controlling bone deposition and resorption. The calculations in this paper support the quantitative feasibility of this fluid shear stress mechanism in osteonal bone formation.

The intriguing feature of the strain-induced fluid shear stresses in the mineralized interior of the osteon near $r = r_m$ is that they exhibit a spectral tuning that provides for a maximum frequency response that could be related to the 20–30 Hz spectral resonance observed in (15,29). Is this fortuitous or does this coincidence serve a special function? As McLeod and Rubin (15) point out, most bone tissue never sees strains of 1,000 μ strain or larger and yet bone tissue is maintained under minimal use. While the origin of the low amplitude 20–30 Hz spectral strain component can be debated, the osteon, if it is to function efficiently as a detector of low-amplitude strain, could optimize this detection capability by having a heightened sensitivity in the same spectral frequency range as this experimentally observed high-frequency strain component. Further, the present analysis predicts that despite the small amplitude of this high frequency strain component (2–4 M Pa), it is of sufficient magnitude to excite a fluid shear-induced intracellular biochemical response in a connected network of osteocytes that act as a neural network to signal other cells to activity. For Curve 5 in Fig. 7 $S(a)_{m,av}$ at 28 Hz would be ~4 dynes/cm^2 for a load of 4 MPa. This is very close to the threshold for the release of intracellular Ca^{++} in (32). Since the location of the maximum shear stress response in the frequency spectrum depends on osteon size (see Fig. 7), it would seem further that the dimensions of the osteon may be determined by either or both the distance that the electrical signal must travel to reach the osteoblasts and the requirement that the osteon optimize its threshold sensitivity for detecting small strains.

In our final remarks, we would like to suggest several functional roles that necessitate the presence of a proteoglycan gel in the fluid annulus of the lacunar-canalicular porosity. First, as observed in Fig. 2, the matrix reduces by more than one order of magnitude the shear stress that would exist on the osteocytic process if it were not present. Second, the microcirculatory blood vessels in bone are known to be significantly more permeable than muscle capillaries. Large amounts of albumin would be lost to the bone tissue unless there were an effective molecular sieve for this molecule in the lacunar-canalicular porosity. In capillaries in muscle tissue this molecular sieve has been demonstrated to exist in a surface glycocalyx at the luminal front of the endothelial cells (1). Third, the presence of proteoglycan proteins serves as an

inhibitor of mineralization, thus enabling the osteocyte to maintain the thin fluid layer that surrounds its membrane (21).

REFERENCES

1. Adamson, R.H.; Clough, G. Plasma proteins modify the endothelial cell glycocalyx of frog mesenteric microvessels. J. Physiol. 445:473–486; 1992.
2. Bianco, P.; Fisher, L.W.; Young, M.F.; Termine, J.D.; Robey, P.G. Expression and localization of the two small proteoglycans, biglycan and decorin, in human developing skeletal and non-skeletal tissues. J. Histochem. Histocytol. 38:1549–1563; 1990.
3. Buckwalter, J.A.; Rosenberg, L.C. Electron microscopic studies of cartilage proteoglycans—Direct evidence for the variable length of the chondroitin sulfate-rich region of proteoglycan subunit core protein. J. Biol. Chem. 257:9830–9839; 1982.
4. Buschmann, M.D.; Basser, P.J.; Grodzinsky, A.J. A microstructural model for swelling pressure and compressive modulus of tissue containing charged GAG chains: Comparison to Donnan theory, Bioengineering Conference. Langrana, N.A.; Friedman, M.H.; Grood, E.S., eds. ASME; 1993: pp. 80–83.
5. Cowin, S.C.; Weinbaum, S.; Zeng, Y. A case for bone canaliculi as the anatomical site of strain generated potentials. J. Biomechanics, in press.
6. Doty, S.B.; Schofield, B.H. Metabolic and structural changes within osteocytes of rat bone in: Talmage, B.V.; Munson, P.L., eds. Calcium, Parathyroid Hormone and the Calcitonins. Amsterdam: Excerpta Medica; 1972: pp. 353–364.
7. Frank, J.S.; Fogelman, A.M. Ultrastructure of the intima in WHHL and cholesterol-fed rabbit aortas prepared by ultrarapid freezing and freeze-etching. J. Lipid Res. 30:967–977; 1989.
8. Jeansonne, B.G.; Eagin, F.F.; McMinn, R.W.; Sheemaker, R.L.; Rehm, W.S. Cell to cell communication of osteoblasts. J. Dental Res. 58:1415–1423; 1979.
9. Johnson, M.W.; Chakkalakal, D.A.; Harper, R.A.; Katz, J.L.; Rouhana, S.W. Fluid flow in bone. J. Biomechanics 11:881–885; 1982.
10. Kamiya, A.; Togawa, T. Adaptive regulation of wall shear stress to flow change in the canine carotid artery. Am. J. Physiol. 239:H14–H21; 1980.
11. Kamiya, A.; Bukhari, R.; Togawa, T. Adaptive regulation of wall shear stress optimizing vascular tree function. Bull. Math. Biol. 46:127–137; 1984.
12. Kufahl, R.H.; Saha, S. A theoretical model for stress-generated fluid flow in the canaliculi-lacunae network in bone tissue. J. Biomechanics 23:171–180; 1990.
13. Langille, B.L.; O'Donnell, F. Reductions in arterial diameter produced by chronic decreases in blood flow are endothelium-dependent. Science 231:405–407; 1986.
14. Lowenstein, W.R. The cell-to-cell channel of gap junctions. Cell 48:725–726; 1987.
15. McLeod, K.J.; Rubin, C.T. Strain oscillations in functionally loaded bone: A species independent determinant of skeletal morphology. J. Biomechanics, in press.
16. Michel, C. Capillary permeability and how it may change. J. Physiol. 404:1–29; 1988.
17. Petrov, N., Pollack, S., and Blagoeva R. A discrete model for streaming potentials in a single osteon. J. Biomechanics 22:517–521; 1989.
18. Piekarski, K.; Munro, M. Transport mechanism operating between blood supply and osteocytes in long bones. Nature 269:80–82; 1977.
19. Prince, C.W.; Rahemtulla, F.; Butler, W.T. Incorporation of [^{35}S]-sulphate into glycosamino-glycans by mineralized tissues *in vivo*. Biochem. J. 224:941–945; 1984.
20. Reich, K.M.; Frangos, J.A. Effect of flow on prostaglandin E_2 and inositol triphosphate levels in osteoblasts. Am. J. Physiol. 261:C428–C432; 1991.
21. Robey, P.G.; Bianco, P.; Termine, J.D. The cellular biology and molecular biochemistry of bone formation. *In* Disorders of Bone and Mineral Metabolism, edited by F.L. Coe and M.J. Favus, New York: Raven Press, 1992, pp. 241–263.
22. Salzstein, R.A.; Pollack, S.R.; Mark, A.F.T.; Petrov, N. Electromechanical potentials in cortical bone-I. A continuum approach. J. Biomechanics 20:261–270; 1987.
23. Salzstein, R.A.; Pollack, S.R. Electromechanical potentials in cortical bone-II. Experimental analysis. J. Biomechanics 20:271–280; 1987.
24. Starkebaum, W.; Pollack, S.R.; Korostoff, E. Microelectrode studies of stress-generated potentials in four-point bending of bone. J. Biomed. Mat. Res. 13:729–751; 1979.
25. Scott, G.C.; Korostoff, E. Oscillatory and step response electromechanical phenomena in human and bovine bone. J. Biomechanics 23:127–143; 1990.
26. Tanaka, T.; Sakano, A. Differences in permeability of microperoxidase and horseradish peroxidase into alveolar bone of developing rats. J. Dental Res. 64:870–876; 1985.
27. Timoshenko, S.P.; Goodier, J.N. Theory of elasticity. New York: McGraw Hill, 1970, 567 pp.
28. Tsay, R.Y.; Weinbaum, S. Viscous flow in a channel with periodic cross-bridging fibers: Exact solutions and Brinkman approximation. J. Fluid Mech. 226:125–148; 1991.
29. Turner, C.H.; Yoshikawa, T.; Forwood, M.R.; Sun, T.C.; Burr, D.B. Functional significance of high frequency components of bone strain in dogs. Trans. ORS 126; 1993.
30. Wassermann, F.; Yaeger, J.A. Fine structure of the osteocyte capsule and of the wall of the lacunae in bone. Zeitschrift für Zellforschung 67:636–652; 1965.
31. Weinbaum, S.; Cowin, S.C.; Zeng, Y. A model for the excitation of osteocytes by mechanical loading induced bone fluid shear stresses. J. Biomechanics 273:339–360, 1994.
32. Williams, J.L.; Iannotti, J.P.; Ham, A.; Bleuit, J.; Chen, J.H. Effects of fluid shear stress in bone cells. J. Biorheol ogy 31:163–170, 1994.

NOMENCLATURE AND VALUES OF PARAMETERS EMPLOYED

a = radius of the osteocytic process.

a_0 = radius of the fiber traversing the annular region between the osteocytic process and the canaliculus wall.

b = radius of the canaliculus.

B = dimensionless constant that is a ratio of the increment in pore water pressure to the increment in the sum of the three normal stresses in the solid matrix ($B = 0.53$).

c = diffusion coefficient in the differential equation governing the pore fluid pressure

d = half the thickness of bone specimen used in experiments ($2d$ = 1 mm).
I_0, I_1, I_2 = modified Bessel functions of the first kind.
K_0, K_1, K_2 = modified Bessel functions of the second kind.
k_p = the cell process channel scale Darcy law permeability constant for fluid flow through the mid-section of a cell process channel filled with transverse fibers.
n = number of channels per unit area; in Cowin *et al.* (5) it is n/L^2, where L is the mean center-to-center distance between two lacunae.
p = pore fluid pressure.
P = dimensionless pressure ($=3p/\sigma BT$).
q = the ratio of the radius of the canaliculus, b, to the radius of the osteocytic process, a.
r_i = radius of the osteonal lumen ($=27$ μm).
R_i = dimensionless radius of the osteonal lumen ($=r_i/r_o = 0.27$).
r_o = radius of the periodic boundary around the osteon.
r_m = mean areal radius ($r_m = \sqrt{(r_o^2 + r_i^2)/2}$)
t = time.
T = dimensionless time ($=\omega r_o^2 c^{-1}$).
T_{ij} = cartesian stress tensor components of the bone matrix.
V_{SGP} = strain generated potential.
$\overline{V}_{SGP}$ = dimensionless strain generated potential.
γ = dimensionless parameter ($=b/\sqrt{k_p}$) that is the ratio of two lengths, the radius of the canaliculus b and the thickness of the fiber-induced viscous layer near the wall, $\sqrt{k_p}$.
Δ = open space between the transverse fibers in the channel between the cytoplasmic process and the wall of the canaliculus.
μ = bone fluid viscosity.
ρ = radial coordinate spanning from the radius of the osteocytic process to the radius of the canaliculus.
σ = the magnitude of the periodic axial compressive stress.
σ_0 = the magnitude of the temporally constant compressive stress.
σ_f = conductivity of the bone fluid.
θ = polar angle in cross-section of osteon.
τ = dimensionless time ($=ctr_o^{-2}$).
$s(a)$ = shear stress acting on the surface of the osteocytic process.
$s(a)_\infty$ = shear stress acting on the surface of the osteocytic process in the very dilute fiber limit.
τ_d = characteristic time of decay of the fluid pore pressure ($=r_o^2 c^{-1}$).
τ_f = characteristic time of applied forcing ($=\omega^{-1}$).
ω = driving frequency.